Optics Communications 333 (2014) 115–119

Contents lists available at ScienceDirect

Optics Communications

journal homepage: www.elsevier.com/locate/optcom

Thermal lensing and laser performance of Tm:LuAG crystal at room temperature

Chunting Wu [a,c,*], Fei Chen [b], Rui Wang [b], Youlun Ju [c]

[a] Jilin Key Laboratory of Solid Laser Technology and Application, School of Science, Changchun University of Science and Technology, Changchun 130022, China
[b] State Key Laboratory of Laser Interaction with Matter, Changchun Institute of Optics, Fine Mechanics and Physics, Chinese Academy of Sciences, Changchun 130033, China
[c] National Key Laboratory of Tunable Laser Technology, Harbin Institute of Technology, Harbin 150001, China

ARTICLE INFO

Article history:
Received 16 March 2014
Received in revised form
19 June 2014
Accepted 7 July 2014
Available online 18 July 2014

Keywords:
Diode-pumped lasers
Tm:LuAG
Thermal lensing

ABSTRACT

In this paper, thermal effect of a diode-end-pumping Tm:LuAG crystal is analyzed and the lasing characteristics at room temperature are also investigated. Based on a thermal model, the thermal focal length of Tm:LuAG crystal is calculated at different pump energies between 50 mJ and 300 mJ. The sensitivity factor of the thermal lens $M=d(1/f)/dP_{abs}$ is estimated to be 0.36 m^{-1}/W or 36 m^{-1}/J. The thermal focal length of Tm:LuAG crystal is also measured at different pump energies. Results show that the experimental data are very well in accordance with the theoretical calculations. Laser characteristics of Tm:LuAG crystal at room temperature are also investigated. Under a pump energy of 300 mJ, the maximum output energy of 41.0 mJ is obtained, with a slope efficiency of 20.8%. The build-up time of the pulse is 2.76 ms, and the beam quality factor is measured to be $M^2=1.17$.

1. Introduction

All-solid-state lasers operating at 2 μm are useful for the applications in coherent Doppler LIDAR, differential absorption LIDAR and so on [1–4]. Thulium-doped $Lu_3Al_5O_{12}$ (Tm:LuAG) crystal is one of the attractive materials, which is isomorphic to YAG [5]. It has not only the advantages of higher heat conductivity, but also the lower population density at the lower laser level. The emission wavelength of Tm:LuAG (2.023 μm) is more closer to the optical transmission window than that of Tm:YAG (2.015 μm).

In 1995, diode-pumped Tm:LuAG laser with an optical-to-optical conversion efficiency of 23.6% was reported [6]. In 2000, an output of 0.92 W diode-pumped Tm:LuAG laser was obtained [7]. In 2004, a single mode Tm:LuAG laser was developed [8]. In 2008, the maximum output power of 4.91 W Tm:LuAG laser with a slope efficiency of 25.39% was obtained [9]. In 2009, a single frequency Tm:LuAG laser was reported with output power of 148 mW [10]. Although the laser characteristics of Tm:LuAG laser had been demonstrated, few research works were carried out on the thermal effect analysis of Tm:LuAG crystal. As a quasi-three-level laser system, the thermal effect of Tm^{3+}-doped crystal could not be ignored. In 2011, Yao et al. [11] reported the thermal analysis of Tm:YLF crystal and Tm:YAP crystal. In 2012, Gaponenko et al. [12] reported the thermal lensing of Tm^{3+}-doped $KY(WO_4)_2$ crystal. The results showed that the thermal effect of Tm^{3+}-doped crystal was quite severe, which would affect the output laser characteristics.

This letter focuses on the analysis of thermal effect about Tm:LuAG crystal and the lasing characteristics of Tm:LuAG at room temperature. The thermal model of Tm:LuAG crystal was built up. And the measured thermal focal length was nearly the same as the calculated value. For example, the thermal focal length of Tm:LuAG crystal was 92.8 mm theoretically and 102.7 mm experimentally under the same conditions of pumping source and the same parameters of laser crystal. Under pump energy of 300 mJ, maximum output energy of 41.0 mJ was obtained, with slope efficiency of 20.8%. The build-up time of the pulse was 2.76 ms. And the beam quality factor was $M^2=1.17$.

2. Thermal effect analysis of Tm:LuAG crystal

2.1. Thermal model

A diagrammatic sketch of diode-end-pumped Tm:LuAG rod is shown in Fig. 1. This model was similar to our previous report [13,14]. In Fig. 1, r and z are the radial and the axial coordinates,

* Corresponding author at: Jilin Key Laboratory of Solid Laser Technology and Application, School of Science, Changchun University of Science and Technology, Changchun 130022, China.
E-mail address: bigsnow1@126.com (C. Wu).

http://dx.doi.org/10.1016/j.optcom.2014.07.027
0030-4018/

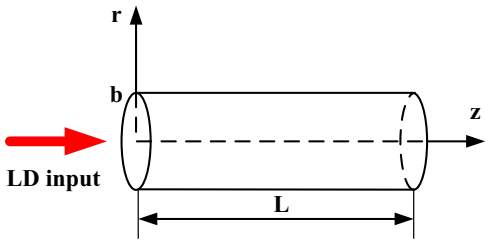

Fig. 1. Model of pulsed laser-diode end-pumped a Tm:LuAG rod.

respectively. b is the radius of rod, and L is the length of rod. Pump light is propagated in the z direction.

Along the z direction, the pump-light-intensity is described by,

$$I(r,z,t)=\frac{2P}{\pi\omega^2}\exp(-2r^2/\omega^2)\exp[-\beta z]G(t),\ 0\le z\le L \tag{1}$$

here, P is the peak power of a pump pulse, ω is the radius of the pump beam waist, and β is the absorption coefficient of Tm:LuAG rod. $G(t)$ is given by,

$$G(t)=[\mathrm{square}(2\pi ft,\tau\cdot f)+1]/2 \tag{2}$$

square is the rectangular square wave function. t is the time and f is the pump repetition rate.

The heat source function is expressed as,

$$q_v(r,z,t)=\beta\eta I(r,z,t)=\frac{2P\beta\eta}{\pi\omega^2}\exp(-2r^2/\omega^2)\exp[-\beta z]G(t) \tag{3}$$

here, η is the heat fraction.

In single pulse duration time, it satisfies the transient heat conduction mode as shown in Eq. (4).

$$\rho c\frac{\partial T_1}{\partial t}=k\left(\frac{\partial^2T_1}{\partial r^2}+\frac{1}{r}\frac{\partial T_1}{\partial r}+\frac{\partial^2T_1}{\partial z^2}\right)+q_v,\ 0\le t\le\tau,\ 0\le z\le L,\ 0\le r\le b \tag{4}$$

The boundary condition is shown in Eqs. (5)–(7).

$$T_1=T_w, r=b \tag{5}$$

$$-k\frac{\partial T_1}{\partial z}+hT_1=hT_e, z=0 \tag{6}$$

$$k\frac{\partial T_1}{\partial z}+hT_1=hT_e, z=L \tag{7}$$

Initial condition is shown in Eq. (8).

$$T_1=T_0,\ t=0,\ 0\le z\le L0\le z\le L,\ 0\le r\le b \tag{8}$$

In single pulse interval time, it satisfies the transient heat conduction mode as shown in Eq. (9).

$$\rho c\frac{\partial T_2}{\partial t}=k\left[\frac{\partial^2T_2}{\partial r^2}+\frac{1}{r}\frac{\partial T_2}{\partial r}+\frac{\partial^2T_2}{\partial z^2}\right],\ \tau\le t\le T,\ 0\le z\le L,\ 0\le r\le b \tag{9}$$

Boundary condition is expressed by Eqs. (10)–(12).

$$T_2=T_w,\ r=b \tag{10}$$

$$-k\frac{\partial T_2}{\partial z}+hT_2=hT_e,\ z=0 \tag{11}$$

$$k\frac{\partial T_2}{\partial z}+hT_2=hT_e,\ z=L \tag{12}$$

The initial condition is given in the Eq. (13).

$$T_2(r,z,t)\big|_{t=\tau}=T_1(r,z,\tau) \tag{13}$$

here ρ is the crystal density, C is the specific heat capacity, h is the heat transfer coefficient of the air, k is the heat conductivity. T_w is the temperature of cooling water. T_e is the initial temperature in the crystal. T_0 is the room temperature.

In the following, an integral transform method is used to get the expressions of T_1 and T_2.

$$T_1(r,z,t)=\sum_{m=1}^{\infty}\sum_{p=1}^{\infty}\frac{R_0(\beta_m,r)Z(\eta_p,z)}{N(\beta_m)N(\eta_p)}e^{-\alpha(\beta_m^2+\eta_p^2)t}\left[\tilde{\bar{T}}_0(\beta_m,\eta_p,t)+\int_{t'=0}^{t}e^{\alpha(\beta_m^2+\eta_p^2)t'}A(\beta_m,\eta_p,t')dt'\right] \tag{14}$$

$$T_2(r,z,t)=\sum_{m=1}^{\infty}\sum_{p=1}^{\infty}\frac{e^{\alpha(\beta_m^2+\eta_p^2)(\tau-t)}}{N(\beta_m)N(\eta_p)}R_0(\beta_m,r)Z(\eta_p,z)\int_{r'=0}^{b}\int_{z'=0}^{L}r'R_0(\beta_m,r')Z(\eta_p,z')T_1(r',z',\tau)dr'dz'+\sum_{m=1}^{\infty}\sum_{p=1}^{\infty}\frac{e^{\alpha(\beta_m^2+\eta_p^2)(\tau-t)}}{N(\beta_m)N(\eta_p)}R_0(\beta_m,r)Z(\eta_p,z)\int_{t'=\tau}^{t}e^{\alpha(\beta_m^2+\eta_p^2)(t'-\tau)}B(\beta_m,\eta_p,t')dt' \tag{15}$$

The unknown variables are described as follows,

$$\tilde{\bar{T}}_0(\beta_m,\eta_p,t)=T_0\int_{z'=0}^{L}\int_{r'=0}^{b}r'R_0(\beta_m,r')Z(\eta_p,z')dr'dz' \tag{16}$$

$$A(\beta_m,\eta_p,t')=\frac{\alpha}{k}\tilde{\bar{q}}_v(\beta_m,\eta_p,t')G(t')+\alpha\frac{Z(\eta_p,z)}{k}\Big|_{z=0}hT_e\pi b^2+\alpha\frac{Z(\eta_p,z)}{k}\Big|_{z=L}hT_e\pi b^2 \tag{17}$$

$$\tilde{\bar{q}}_v(\beta_m,\eta_p,t')=\int_{z'=0}^{L}\int_{r'=0}^{b}rR_0Z(\eta_p,z')q_v(r',z',t')dr'dz' \tag{18}$$

$$B(\beta_m,\eta_p,t')=\alpha\frac{Z(\eta_p,z)}{k}\Big|_{z=0}hT_e\pi b^2+\alpha\frac{Z(\eta_p,z)}{k}\Big|_{z=L}hT_e\pi b^2 \tag{19}$$

$$R_0(\beta_m,r)=J_0(\beta_m r) \tag{20}$$

$$\frac{1}{N(\beta_m)}=\frac{2}{b^2J_0^2(\beta_m b)} \tag{21}$$

here, $J_0(\beta_m r)$ is the zero order Bessel function. Eigenvalue β_m is the positive root of the equation $J_0(\beta_m b)=0$.

$$Z(\eta_p,z)=\eta_p\cos\eta_p z+(h/k)\sin\eta_p z \tag{22}$$

$$\frac{1}{N(\eta_p)}=\frac{2}{[\eta_p^2+(h/k)^2]\left[L+\frac{(h/k)}{\eta_p^2+(h/k)^2}\right]+(h/k)} \tag{23}$$

here, η_p is the positive root of the equation $\tan\eta_pL=(\eta_p(h/k+h/k)/\eta_p^2-(hh/kk))$.

After n $(n\ge2)$ pump pulses, the expression of temperature distribution in repeated pulse duration time could be given as follows:

$$T_{2n-1}(r,z,t)=\sum_{m=1}^{\infty}\sum_{p=1}^{\infty}\frac{R_0(\beta_m,r)Z(\eta_p,z)}{N(\beta_m)N(\eta_p)}e^{-\alpha(\beta_m^2+\eta_p^2)[t-(n-1)T]}\int_{r'=0}^{b}\int_{z'=0}^{L}r'R_0(\beta_m,r')Z(\eta_p,z')\cdot T_{2n-2}(r',z',nT-T)dr'dz'+\sum_{m=1}^{\infty}\sum_{p=1}^{\infty}\frac{R_0(\beta_m,r)Z(\eta_p,z)}{N(\beta_m)N(\eta_p)}e^{-\alpha(\beta_m^2+\eta_p^2)[t-(n-1)T]}\cdot\int_{t'=(n-1)T}^{t}e^{\alpha(\beta_m^2+\eta_p^2)[t'-(n-1)T]}A(\beta_m,\eta_p,t')dt' \tag{24}$$

After it is pumped by $n(n \geq 2)$ pulses, the temperature distribution in repeated pulse interval time is given by

$$T_{2n}(r,z,t) = \sum_{m=1}^{\infty}\sum_{p=1}^{\infty} \frac{R_0(\beta_m,r)Z(\eta_p,z)}{N(\beta_m)N(\eta_p)} e^{-\alpha(\beta_m^2+\eta_p^2)[t-\tau-(n-1)T]} \int_{r'=0}^{b} \int_{z'=0}^{L} r' R_0(\beta_m,r')Z(\eta_p,z') \cdot T_{2n-1}(r',z',\tau+nT-T)dr'dz' + \sum_{m=1}^{\infty}\sum_{p=1}^{\infty} \frac{e^{-\alpha(\beta_m^2+\eta_p^2)[t-\tau-(n-1)T]}}{N(\beta_m)N(\eta_p)} R_0(\beta_m,r)Z(\eta_p,z) \cdot \int_{t'=\tau+(n-1)T}^{t} e^{\alpha(\beta_m^2+\eta_p^2)[t'-\tau-(n-1)T]} B(\beta_m,\eta_p,t')dt' \quad (25)$$

In the rod, the thermally induced optical path difference (OPD) is induced by the change of refractive index with temperature [15]. The OPD in the slice z to dz is given by

$$d\mathrm{OPD}(r,z,t) = \left[\frac{dn}{dT} + (n-1)(\upsilon+1)\alpha_T\right] \times [T(0,z,t) - T(r,z,t)]dz \quad (26)$$

The thermal focal length varied with time is expressed as

$$f = \frac{r_e^2}{2\mathrm{OPD}} = \frac{r_e^2}{2\left\{\left[\frac{dn}{dT} + (n-1)(\upsilon+1)\alpha_T\right] \times \int_a^L [T(0,z,t) - T(r_b,z,t)]dz\right\}} \quad (27)$$

here r_e is the effective radius of pump light.

2.2. Simulation results and analysis

The parameters used in simulation is shown in Table 1.

The transient temperature distribution and the time-varying thermal focal length in Tm:LuAG crystal are shown in Figs. 2 and 3 .

As shown in Fig. 2, the temperature distribution appeared jagged with time. The maximum temperature of Tm:LuAG crystal arrived at 72.7°C. And the interval that axially transient temperature distribution reached steady state is 1.2 s. In Fig. 3, the time-varying thermal focal length appeared jagged and decreased with time. The thermal focal length is in the range of 92.8–381.0 mm. At pump peak power of 30 W, pump frequency of 50 Hz and pump pulse duration of 10 ms, the thermal focal length is 381.0 mm at the beginning and stable at 92.8 mm after about 120 pumped-cycles. From Figs. 2 and 3, it was obvious that although the pumping source was a pulsed laser diode, the temperature distribution and focal lens of thermal lensing stabilized to a steady state while pump time continued.

Table 1
Parameters used in simulation.

Parameters	Value
Temperature of cooling liquid/K	291
Initial temperature/K	295
Heat transfer coefficient of air/(W cm^{-2} K^{-1})	8×10^{-4}
Heat conductivity of Tm:LuAG/(W cm^{-1} K^{-1}) [16]	0.079
Pump beam waist/cm	0.12
Pump peak power/W	30
Pump frequency/Hz	50
Pump pulse duration/ms	10
Heat fraction	0.6
Crystal radius/mm	1.5
The length of Tm:LuAG rod/mm	8
Density of Tm:LuAG/(g/cm^3) [16]	6.32
Specific heat capacity of Tm:LuAG/(J Kg^{-1} K^{-1}) (similar to Tm:YAG)	590
Absorption coefficient of 4 at% Tm:LuAG/cm^{-1}	3
Thermo-optical coefficient $(dn/dT)/(K^{-1})$ [16]	8.9×10^{-6}
Refractive index of Tm:LuAG rod	1.81
Poisson's ratio	0.3
Thermal expansion coefficient/(K^{-1}) [16]	7.9×10^{-6}

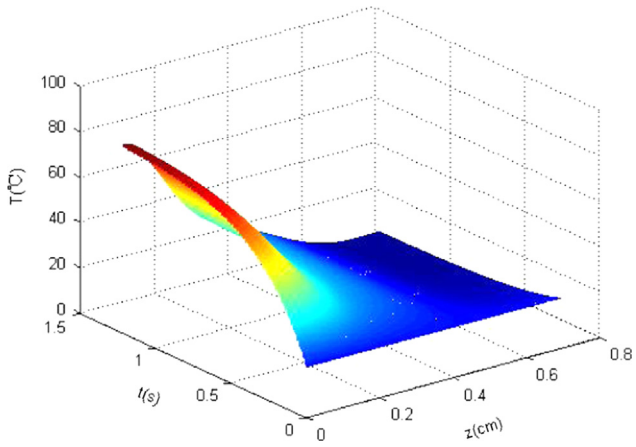

Fig. 2. Axially transient temperature distribution in Tm:LuAG crystal.

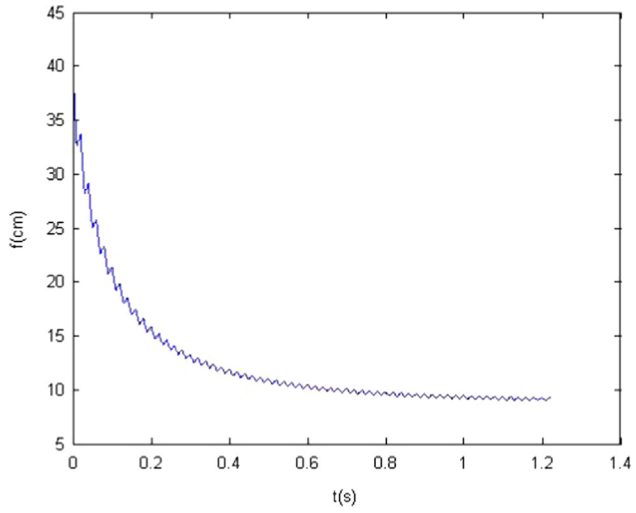

Fig. 3. Thermal focal length in Tm:LuAG crystal versus time.

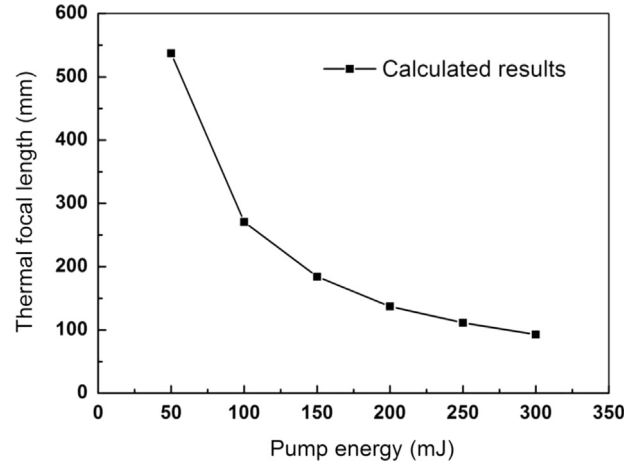

Fig. 4. Thermal focal length versus pump energy.

Fig. 4 gave the thermal focal length of Tm:LuAG crystal under different pump energies (pump peak power × Pump pulse duration). And the sensitivity factor of the thermal lens $M = d(1/f)/dP_{abs}$ was about 0.36 m^{-1}/W or 36 m^{-1}/J. The smaller the pump spot radius was, the shorter the thermal focal length became. Therefore, the value of M would be bigger, which meant that the laser crystal would be more sensitive to the thermal effect.

3. Experimental setup

Fig. 5 shows the experimental setup of the Tm:LuAG laser. The oscillator was a bowtie cavity in a bidirectional fashion. The pump source was pulsed fiber-coupled laser-diode (LD) with a peak power of 30 W and central wavelength of 788 nm. The frequency and the pulse duration of the LD was 50 Hz and 10 ms, respectively. The fiber core had a diameter of 400 μm and a numerical aperture of 0.22. The output beam of the laser-diode was collected by 25 mm focal length collimating lens, and it was focused into the Tm:LuAG crystal using a lens with 75 mm focal length. Then, the radius of pumping beam waist was 0.6 mm. The Tm:LuAG laser crystal had a Tm-doped concentration of 4%, with the dimensions of $\Phi 3 \times 8$ mm^3. Both sides were coated antireflection near 788 nm ($R < 0.5\%$) and 2.02 μm ($R < 0.5\%$). The temperature of the crystal was kept at 291 K with a TE-cooler. The resonator was designed to be insensitive to the thermal lens of Tm:LuAG crystal by considering the thermal focal length, as calculated above. The radius of oscillating beam (ω) would be changed because of the thermal effect of Tm:LuAG crystal. And the stability of the cavity would turn to bad. Therefore, the $d\omega/df$ was introduced as an important factor to characterize whether a cavity was designed successfully. The $d\omega/df$ for our experiment was approximate equal to 0 unless the thermal lens was shorter than 80 mm. M1 was a high-reflectivity flat mirror. M2 was a flat output coupler with a transmission of 3.5% at 2.02 μm. M3 and M4 were curved mirrors with 5 m radius of curvature and coated with high-reflectivity at 2.02 μm. The total resonator length was 0.3 m.

4. Experimental results and discussion

The output energy of Tm:LuAG laser was measured by an energy meter, as shown in Fig. 6. The threshold of the laser was 95.3 mJ. The maximum output energy was 41.0 mJ with pump energy of 300 mJ. The slope efficiency was 20.8%. There is no saturation phenomenon of Tm:LuAG output energy. It meant that the cavity-design was successful.

The output laser was detected by an InGaAs detector connected with a digital oscilloscope (Tektronix TDS3032B). The build-up time of the pulse was 2.76 ms when the pump energy was 300 mJ, as shown in Fig. 7.

At the maximum output energy, a beam quality factor of $M^2 = 1.17$ was measured by the traveling knife-edge method. By the way of the lens-transformation, as shown in Fig. 8, we could know the position of the beam waist and the beam divergence angle in the resonator, according to the following equations:.

$$\omega_0' = \frac{F}{\sqrt{(1-F)^2 + f^2}}\omega_0 \tag{28}$$

$$l' = F + \frac{(l-F)F^2}{(1-F)^2 + f^2} \tag{29}$$

where, f is the confocal parameter, $f = \pi\omega_0^2/\lambda$. l or l' is the distance between the lens and the waist in the cavity or outside the cavity. F is the focal length of the lens.

The position and the radius of the beam waist in the cavity would be different by considering or ignoring the thermal lens of the Tm:LuAG crystal. This difference should disappear by changing the value of the thermal focal length. However, it was a huge amount of calculation.

Based on the similar principles, by means of software about LasCAD, the thermal focal length could be defined easily. Specifically, the position of the beam waist and the beam divergence angle in the cavity could be determined when designing the resonator. Supposing a thermal lens, changing the value of the thermal focal length, then the position of the beam waist and the beam divergence angle in the cavity would be changed

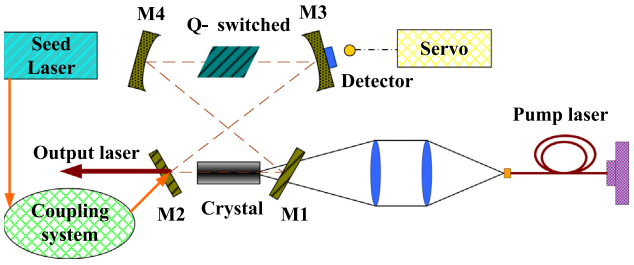

Fig. 5. Schematic of the Tm:LuAG laser.

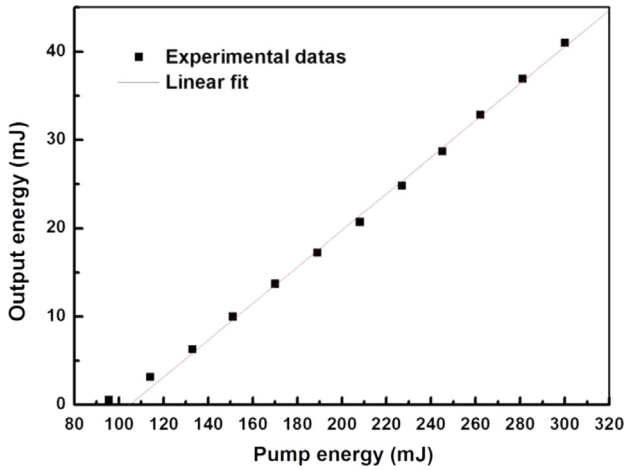

Fig. 6. Output energy versus pump energy.

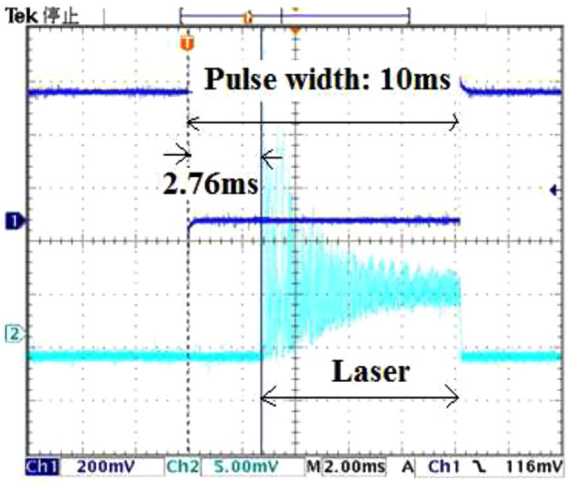

Fig. 7. Output laser versus time.

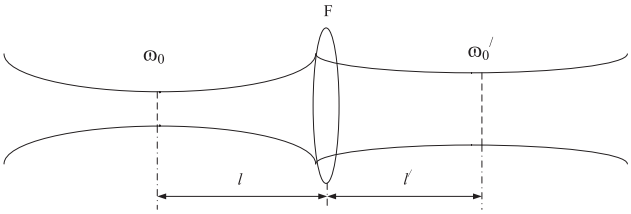

Fig. 8. Beam waist transformation by the lens.

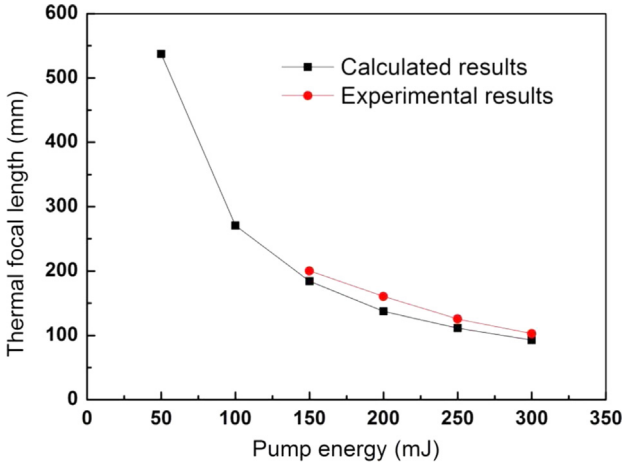

Fig. 9. Thermal focal length versus pump energy.

corresponding. The value of the thermal focal length changed until the position of the beam waist and the beam divergence angle in the resonator was the same with the measuring values. The thermal focal length determined by the above method was named as experimental results.

The thermal focal length of Tm:LuAG crystal was 102.7 mm at pump energy of 300 mJ (pump peak power of 30 W × pulse duration of 10 ms) and frequency of 50 Hz. By this method, the value of thermal focal length could be identified at pump energy of 150 mJ, 200 mJ and 250 mJ. Fig. 9 gave the calculated results and experimental results about thermal focal length versus pump energy. The experimental results coincide with the theoretical calculations. The deviation might due to the missing parameters of Tm:LuAG crystal.

5. Summary

In summary, we reported an analysis of thermal effect about Tm:LuAG crystal and its lasing characteristics at room temperature.

Based on the thermal model of Tm:LuAG crystal, the thermal focal length was estimated theoretically. By means of software about LasCAD, the thermal focal length was also defined from experimental results. The experimental results coincide with the theoretical calculations. The deviation might due to the missing parameters of Tm:LuAG crystal. Under pump energy of 300 mJ, maximum output energy of 41.0 mJ was obtained, with slope efficiency of 20.8%. The build-up time of the pulse was 2.76 ms. And the beam quality factor was $M^2 = 1.17$.

Acknowledgments

This work is supported by Science and Technology Department of Jilin Province in China (No.2012011113).

References

[1] Y.F. Li, B.Q. Yao, Z.G. Wang, Y.Z. Wang, Y.L. Ju, Chin. Opt. Lett. 4 (2006) 470.
[2] B.Q. Yao, L.Q. Dong, Y.Z. Wang, Y.L. Ju, X. Yu, W.F. Sun, Y.F. Li, Acta Opt. Sin. 24 (2004) 79.
[3] J. Yu, B.C. Trieu, E.A. Modlin, U.N. Singh, M.J. Kavaya, S. Chen, Y. Bai, P.J. Petzar, Opt. Lett. 31 (2006) 462.
[4] C. Nagasawa, T. Suzuki, H. Nakajima, H. Hara, K. Mizutani, Opt. Commun. 200 (2001) 315.
[5] J.D. Kmetec, T.S. Kubo, T.J. Kane, C.J. Grund, Opt. Lett. 19 (1994) 186.
[6] N.P. Barnes, M.G. Jani, R.L. Hutcheson, Appl. Opt. 34 (1995) 4290.
[7] V. Wulfmeyer, M Randall, A. Brewer, R.M. Hardesty, Opt. Lett. 25 (2000) 1228.
[8] K. Scholle, E. Heumann, G. Huber, Laser Phys. Lett. 1 (2004) 285.
[9] C.T. Wu, Y.L. Ju, Y.F. Li, Z.G. Wang, Y.Z. Wang, Chin. Opt. Lett. 6 (2008) 415.
[10] C.T. Wu, Y.L. Ju, Q. Wang, Z.G. Wang, F. Chen, R.L. Zhou, Y.Z. Wang, Laser Phys. Lett. 6 (2009) 707.
[11] B.Q. Yao, P.B. Meng, G. Li, Y.L. Ju, Y.Z. Wang, J. Opt. Soc. Am. B 28 (2011) 1866.
[12] M.S. Gaponenko, P.A. Loiko, N.V. Gusakova, K.V. Yumashev, N.V. Kuleshov, A.A. Pavlyuk, Appl. Phys. B 108 (2012) 603.
[13] G.Y. Jin, J. Wu, C.T. Wu, E.H. Fan, C. Wang, X.Y. Chen, Y.J. Yu, X.C. Tan, Chin. J. Lasers 40 (2013) (1002002-1).
[14] J. Wu, C.T. Wu, E.H. Fan, C. Wang, X.Y. Chen, Y.J. Yu, G.Y. Jin, Proc. SPIE 8904 (2013) (890413-1).
[15] X.L. Song, B.B. Li, S.Y. Wang, D.F. Cai, J.G. Wen, Z. Guo, Chin. J. Lasers 34 (2007) 1476.
[16] X.D. Wang, X.D. Xu, T.C. Zang, C.L. Ma, Z.W. Zhao, J. Xu, Chin. J. Rare Earth Soc. 27 (2009) 745.